

Fe–Ni Nanostructures and C/Fe–Ni Composites as Adsorbents for the Removal of a Textile Dye from Aqueous Solution

Jésica Trujillo-Reyes · Marcos Solache-Ríos ·
Alfredo R. Vilchis-Nestor ·
Víctor Sánchez-Mendieta · Arturo Colín-Cruz

Received: 11 March 2011 / Accepted: 6 September 2011 / Published online: 21 September 2011
© Springer Science+Business Media B.V. 2011

Abstract Novel adsorption materials—Fe–Ni nanostructures and C/Fe–Ni composites—with the carbonaceous material coming from sewage sludge, have been developed and evaluated to remove indigo carmine from aqueous solution. The adsorbents were characterized by transmission and scanning electron microscopy, X-ray powder diffraction, IR spectroscopy and Brunauer–Emmett–Teller analysis. Sorption kinetics and isotherms were determined and the adsorption behaviours analysed. All adsorbents here studied have exhibited good efficiency to remove indigo carmine from aqueous solution. Pseudo-second-order kinetic and Langmuir–Freundlich isotherm models were successfully applied to

the experimental data. Fe–Ni nanostructures adsorption capacity was 977.18 mg/g, followed by C/Fe–Ni 75/25% composite with 654.33 mg/g, and a lowest value, 486.41 mg/g, was obtained for C/Fe–Ni 95/5% composite. It can be suggested that the sorption mechanism of the dye is chemisorption on these heterogeneous novel, cheap and efficient functional materials. All materials provide the highest adsorption capacities in pH between 4 and 10. In addition, three sorption–desorption cycles using 30% H₂O₂ solution and distilled water were performed; sorption efficiencies of both composites (C/FeNi 75/25% and C/FeNi 95/5%) decreases in each cycle, but this behaviour is not observed for FeNi nanoscale oxides.

J. Trujillo-Reyes (✉) · V. Sánchez-Mendieta ·
A. Colín-Cruz
Facultad de Química,
Universidad Autónoma del Estado de México,
Paseo Colón y Tolloca s/n,
CP 50000 Toluca, Estado de México, Mexico
e-mail: jtrujillor@uaemex.mx
URL: <http://www.uaemex.mx/>

M. Solache-Ríos
Departamento de Química,
Instituto Nacional de Investigaciones Nucleares,
A.P. 18-1027, Col. Escandón, Delegación Miguel Hidalgo,
C.P. 11801 México D.F., Mexico

A. R. Vilchis-Nestor
Centro de Investigación en Química
Sustentable UAEM–UNAM,
Carretera Toluca–Atlacomulco km 14.5, San Cayetano,
CP 50200 Toluca, Estado de México, Mexico

Keywords Metallic nanostructures · Sewage sludge ·
Textile dyestuff · Aqueous solution

1 Introduction

Many industries, such as dyestuffs, textile, paper and plastics, use dyes in order to colour their products and also consume considerable volumes of water. The presence of very small amounts of dyes in water is visible and undesirable (Forgacs et al. 2004; Banat et al. 1996; Robinson et al. 2002). Due to large-scale production and extensive application, synthetic dyes can cause significant environmental pollution and serious health-risk factors. Indigo carmine is used extensively as a dye by the textile industry, particularly

for denim products. A significant fraction of the remaining indigo is discharged into the environment by hundreds of textile and dyeing factories (Slokar and Le Marechal 1998; Vautier et al. 2001). Indigo carmine dye is considered a highly toxic indigoid class of dye, and its touch can cause skin and eye irritations to human beings, but the consumption can also prove fatal. Thus, keeping the toxicity of this dye in view, various attempts have been made for the removal of indigo carmine from wastewater (Mittal et al. 2006). General methods of decolourizing wastewater are mainly coagulation, membrane separation process, dilution, filtration, Fenton, ozone, TiO_2/UV , enzymes, etc. (Baldrian et al. 2006; Guivarch et al. 2003; Kunwar et al. 2003; Ma et al. 2004; Mc Callum et al. 2000). However, adsorption systems are rapidly gaining prominence as treatment processes which produce high-quality effluents that are low in concentration of dissolved organic compounds, such as dyes (Forgacs et al. 2004; Walker and Weatherle 1997). Recently, numerous approaches have been studied for the development of cheaper and effective adsorbents. Many non-conventional low-cost adsorbents, including natural materials, biosorbents and waste materials from industry and agriculture, have been proposed by several researchers (Crini 2006; Gupta and Suhas 2009; Gutiérrez-Segura et al. 2009; Otero et al. 2003; Torres-Pérez et al. 2008; Trujillo-Reyes et al. 2010; Wang et al. 2008). On the other hand, metallic nanoparticles are beginning to receive more attention because of their relatively higher chemical activity and specificity of interaction. Control of nanoparticle size, shape and dispersity is the key to selective and enhanced activity (White et al. 2008). Nanoscale iron particles represent a new generation of environmental remediation technologies that could provide low-cost, effective solutions to some of the most challenging environmental cleanup problems. Modified iron nanoparticles, such as catalyzed and supported nanoparticles, have been synthesized to further enhance the speed and efficiency of remediation (Trujillo-Reyes et al. 2010; Bokare et al. 2007; Zhang 2003). Moreover, the fusion between porous materials and nanoparticles technology is potentially one of the most interesting and fruitful areas of interdisciplinary research in water treatments. Thus, the aim of this work was to obtain and characterize novel materials of Fe–Ni nanostructures and C/Fe–Ni composites and evaluate their sorption properties to remove indigo carmine from aqueous solution.

2 Experimental

2.1 Materials

2.1.1 Indigo Carmine Dye

In this study, indigo carmine (5,5-indigosulfonic acid, acid blue 74) was obtained as a commercial dye (denim blue) from Mariposa colorants®. It has two sulphonate groups, a molar mass of 466.35 g/mol, colour index number 73,015 and a maximum light absorption at $\lambda_{\text{max}} = 587 \text{ nm}$.

2.1.2 Carbonaceous Material from Sewage Sludge

Sludge was obtained from a wastewater treatment plant in Lerma, Estado de México, Mexico. The complete procedure of sewage sludge thermal treatment has been described elsewhere (Torres-Pérez et al. 2008). Carbonaceous material was washed with distilled water, dried at 60°C for 2 days, crushed and sieved (no. 20, 0.84 mm).

2.1.3 Preparation of Fe–Ni Nanostructures and C/Fe–Ni Composites

Preparations of Fe–Ni bimetallic nanostructures (75/25 wt.% ratio) and both C/Fe–Ni composites (75/25 and 95/5 wt.%) were carried out by sodium borohydride reduction of $\text{FeSO}_4 \cdot 7\text{H}_2\text{O}$ and $\text{NiSO}_4 \cdot 6\text{H}_2\text{O}$ aqueous mixture. Solution of Fe^{2+} and Ni^{2+} ions, together with the carbonaceous material (composites case), was stirred for 10 min, followed by reduction using NaBH_4 . During the reduction reaction, solution colour changed from orange-green to black with formation of dark colloidal particles. The solution was stirred for additional 10 min, followed by vacuum filtration. The particles were rinsed thoroughly with distilled water and acetone and then air-dried overnight for 24 h.

2.2 Characterization

2.2.1 TEM Observations

After drying, Fe–Ni nanoparticles were suspended in 2-propanol using an ultrasonic instrument. TEM samples were prepared by placing a drop of the alcoholic suspension on carbon-coated copper grids. TEM obser-

vations were performed on a transmission electron microscope JEOL-2010, operated at an accelerating voltage of 200 kV equipped with a LaB₆ filament.

2.2.2 X-ray Diffraction

X-ray powder diffraction (XRD) patterns were collected on Bruker X-ray diffractometer model D-8 Advance, equipped with Linxeye detector and source of Cu K α radiation ($\lambda=0.1544$ nm).

2.2.3 SEM/EDS Observations

Scanning electron microscopy (SEM) observations of C/Fe–Ni composites before and after dye sorption were performed by using a JEOL 8810LV electron microscope at 20 kV with 3 nm of resolution. Microanalyses were done with an energy X-ray dispersive spectroscopy (EDS) system.

2.2.4 Brunauer–Emmett–Teller Analysis

Brunauer–Emmett–Teller (BET) surface areas were determined by standard multipoint techniques of nitrogen adsorption, using a BELSORP-max instrument. Samples were heated at 200°C for 2 h before specific surface areas were measured.

2.2.5 IR Analysis

IR spectra of all adsorbent materials before and after sorption process were measured from 4,000 to 800 cm⁻¹ range at room temperature using a Shimadzu Prestige-21 FTIR.

2.3 Sorption Experiments

All batch adsorption experiments were performed in duplicate using a rotating system set at 25 rpm, where 10 mL of indigo carmine solution was added to 10 mg of each adsorbent material, monitoring pH data before and after the experiments at room temperature. For kinetics, each material was in contact during 1, 5, 15, 30, 60, 120, 180, 300, 420 and 600 min with a 100 mg/L indigo carmine solution; isotherms were carried out using 50, 100, 300, 400, 500, 700, 900, 1,000 and 1,300 mg/L of dye solution stirring during 180, 240 and 360 min for Fe–Ni nanostructures, C/Fe–Ni 75/25 wt.% and 95/5 wt.% composites,

respectively. Also, indigo carmine solutions at different pH values of 1, 3, 5, 7, 9, 11 and 13 were tested. Each mixture solution was vacuum filtrated, and dye concentrations were determined in the liquid phases at $\lambda=587$ nm using a PerkinElmer Lambda 25 UV/Vis spectrophotometer. Finally, all materials saturated with indigo carmine dye were left in contact with 30% H₂O₂ solution and distilled water for 24 h. After this treatment, all materials were left in contact a second time with an indigo carmine dye solution at equilibrium time, the phases were separated and dye concentration in each solution was determined as described above; three sorption–desorption cycles were performed.

3 Results and Discussion

3.1 Materials

Carbonaceous material was obtained satisfactorily by pyrolysis of sewage sludge. Moreover, preparation of Fe–Ni nanoparticles and C/Fe–Ni composites were obtained adequately by chemical reduction method. All materials were characterized using TEM, XRD, SEM/EDS, IR and BET.

3.2 Characterization

3.2.1 Transmission Electron Microscopy

Figure 1 displays the TEM images of Fe–Ni nanostructures produced from a 75/25 wt.% mixture of Fe⁺²/Ni⁺² aqueous solution. TEM micrograph in Fig. 1a reveals sheet-like particles as the main morphology. However, higher magnifications images (Fig. 1b, c) show also needle-shaped nanostructures with dimension of about 10–20 nm of diameter, short axis and aspect ratio below 20 nm, while circa 200-nm-long nanorods are also observable.

3.2.2 X-ray Diffraction

The XRD pattern can be indexed to stoichiometric FeNi₃ alloy (JCPDS 65-3244) with a cubic structure (Liao et al. 2006); however, iron oxides are also detected. Presence of other impurities is also possible due to the reduction of nickel by borohydride; in addition to the formation of elemental nickel, Ni₂B

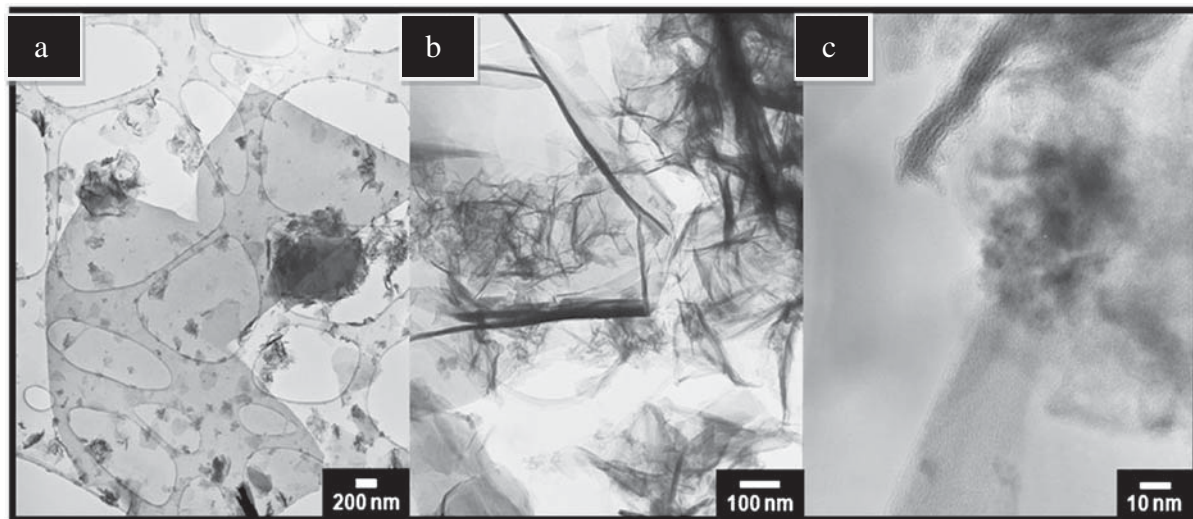


Fig. 1 TEM images of Fe–Ni nanostructures at different scales

and insoluble boron species have also been reported as products in this complex reduction process (Tee et al. 2005). FeNi_3 , ICDD file card no. 38-419; $\text{Fe}_3\text{Ni}_3\text{B}$, ICDD file card no. 36-979; and $\text{Fe}_{4.5}\text{Ni}_{18.5}\text{B}_6$, ICDD file card no. 19-613, along with the expected nickel borides and iron boride (Fe_2B , ICDD file card no. 39-1314), were also detected.

3.2.3 Scanning Electron Microscopy

SEM images of C/Fe–Ni 75/25 wt.% and C/Fe–Ni 95/5 wt.% composites are shown in Fig. 2a, b, respectively. In both images, a rough material with small pores can be observed. SEM images in Fig. 2c, d show each adsorbent material after being in contact

Fig. 2 SEM image of **a** C/Fe–Ni 75/25% and **b** C/Fe–Ni 95/5% composites, and **c** C/Fe–Ni 75/25% and **d** C/Fe–Ni 95/5% composites after indigo carmine adsorption

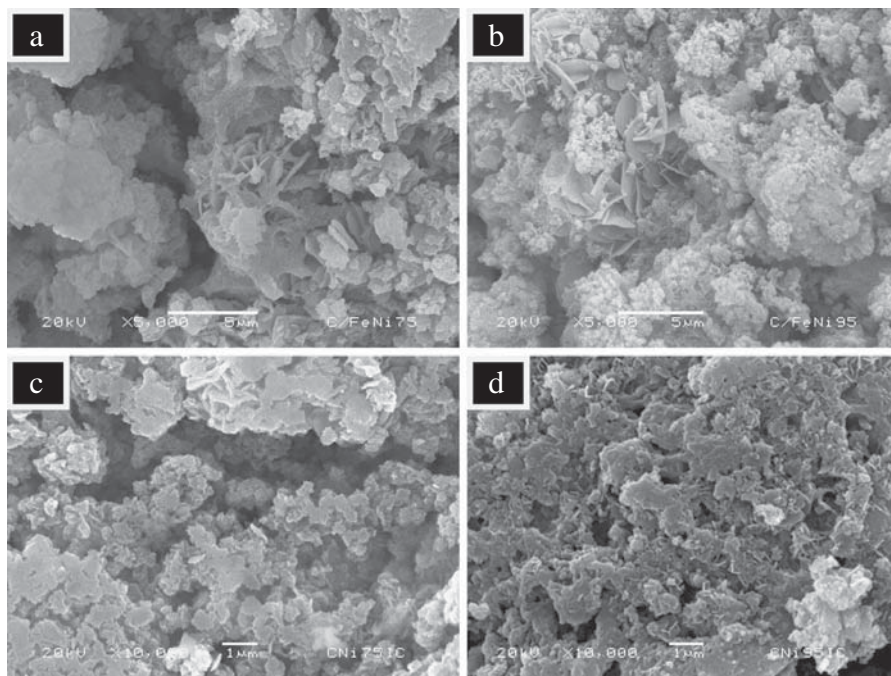


Table 1 Elemental analysis before and after sorption experiments for Fe–Ni nanostructures and C/Fe–Ni composites

Element	Before sorption		After sorption	
	Weight percent Fe–Ni	Weight percent C/Fe–Ni 75/25%	Weight percent Fe–Ni	Weight percent C/Fe–Ni 75/25%
Fe	56.52±2.51	27.39±6.02	46.89±0.81	32.34±2.41
Ni	13.89±1.19	6.14±2.66	11.95±0.02	8.30±1.59
O	29.59±1.32	27.88±5.34	27.56±0.46	29.79±0.20
C		27.75±4.16	13.60±1.25	25.10±3.94
Si		7.25±0.10		2.97±0.27
Al		1.48±0.06		0.87±0.03
Ca		1.85±0.29		0.63±0.05
K		0.52±0.01		
Na		0.54±0.10		
				Weight percent C/Fe–Ni 95/5%
				15.24±0.37
				4.53±0.95
				31.04±1.59
				38.29±0.64
				6.53±0.83
				1.57±0.19
				1.75±0.59
				0.29±0.05
				0.33±0.03

with indigo carmine solution. The four images are similar exhibiting a porous and rough morphology. Chemical analysis was carried out in two different areas at 500× for each adsorbent material. Table 1 shows the EDS analysis for Fe–Ni nanostructures and C/Fe–Ni composites. The nanomaterials were made of 75% Fe and 25% Ni weight ratio; however, it was found that oxygen appears on the elemental composition of the sample. For both composites, EDS indicates a heterogeneous and complex composition, where carbon appears in a bigger proportion, followed by oxygen and silicon, iron and nickel, and others such as aluminium and calcium. This mixture of elements is due to the original composition of sewage sludge carbonaceous material. EDS results after the indigo carmine sorption were comparable to those obtained before the adsorption experiments, which proves the physical and chemical stabilities of these low-cost and efficient composite materials.

3.2.4 BET Analysis

The BET surface areas for Fe–Ni nanostructures and C/Fe–Ni 75/25% and C/Fe–Ni 95/5% composites were 134.11, 70 and 34.25 m²/g, respectively. These results show that increasing the percentage of nanoparticles in the samples, the specific area also increases, and therefore the sorption capacities of these materials in the removal of indigo carmine from aqueous solutions increases.

3.2.5 IR Analysis

The IR spectrum of indigo carmine as a commercial dye (denim blue) from Mariposa colorants® (Fig. 3) exhibits an absorption band at approximately 3,450 cm⁻¹ that corresponds to N–H group. Bands appearing from 2,950 to 2,870 cm⁻¹ correspond to C–H asymmetrical and symmetrical stretching aromatic groups. Also, the band near 1,600 cm⁻¹ corresponds to C=C, C=O aromatic groups. Finally, bands from 1,300 to 1,000 cm⁻¹ region correspond to C–C, N–H and S=O bonds.

IR spectra of each material studied, after they were in contact with indigo carmine solution, are similar and can be compared with those obtained before the adsorption process. The spectra do not show the characteristic bands of the dyestuff spectrum; this behaviour could be due to the low quantity of solute compared to the adsorbent.

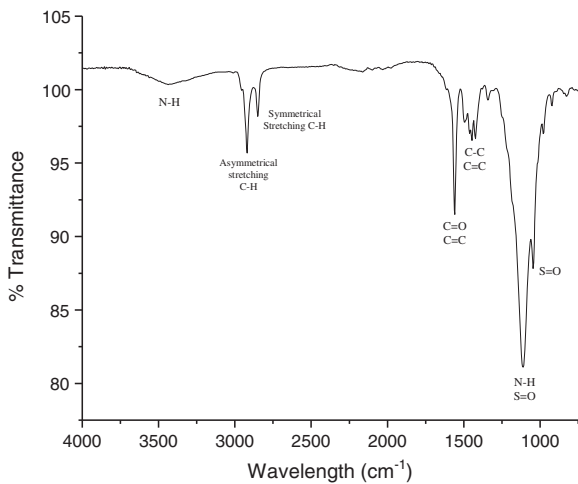


Fig. 3 IR spectrum of indigo carmine as a commercial dye (denim blue) from Mariposa colorants®

3.3 Kinetic Models

Figure 4 shows the kinetic sorption behaviour of indigo carmine by Fe–Ni nanostructures and both C/Fe–Ni composites. The equilibrium time for C/Fe–Ni 95/5% composite was reached in 360 min, for C/Fe–Ni 75/25% composite in 210 min and the equilibrium time for Fe–Ni was reached in 180 min. In these plots, there are three different portions, representing the different stages in adsorption, an initial curved portion followed by a linear portion and then a plateau. The initial curve segment is due to surface adsorption and rapid external diffusion (boundary layer diffusion). The second linear part is the gradual adsorption stage where the intra-particle diffusion is rate-controlled. The plateau (third portion) is the final equilibrium

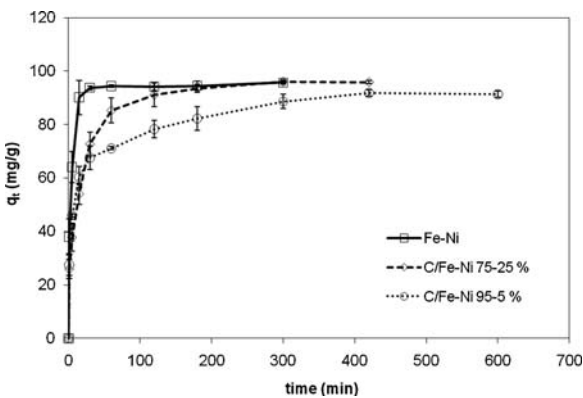


Fig. 4 Kinetics of Fe/Ni nanostructures and C/Fe–Ni composites

Table 2 Kinetic and sorption isotherm parameters of indigo carmine sorption by Fe–Ni nanostructures and C/Fe–Ni composites

Material	Lagergren		Kinetic models		Ho and McKay		
	q_e (mg/g)	K_L (h^{-1})	r^2	a (mg/g)	b (mg/g)	r^2	
Fe–Ni	93.39	0.302	0.985	1566.09	0.102	0.966	
C/Fe–Ni 75/25%	91.73	0.068	0.967	80.07	0.076	0.988	
C/Fe–Ni 95/5%	80.90	0.146	0.941	200.13	0.099	0.997	
Material	Langmuir		Sorption isotherms		Langmuir–Freundlich		
	q_0 (mg/g)	b	r^2	K_F (mg/g)(L/mg) ^{1/n}	n	r^2	
Fe–Ni	977.18	0.012	0.931	53.60	2.096	0.932	
C/Fe–Ni 75/25%	654.33	0.020	0.992	79.77	3.004	0.977	
C/Fe–Ni 95/5%	486.41	0.009	0.981	41.18	2.764	0.952	
		Langmuir		Freundlich		Ho and McKay	
		K	r^2	q_e (mg/g)	K (g/mg h)	r^2	n
		30.88	0.934	96.15	0.0081	0.999	1.427
		21.77	0.993	97.08	0.0014	0.999	1.177
		30.78	0.995	92.59	0.0010	0.998	2.103

stage, where the intra-particle diffusion starts to slow down due to the low solute concentration in solution (Crini and Badot 2008). At the equilibrium, the amount of indigo carmine dye on all adsorbent materials, q_e (milligrams per gram), was found by a mass balance relationship:

$$q_e = (C_o - C_e)V/W \quad (1)$$

where C_o (milligrams per litre) and C_e (milligrams per litre) are the initial and the equilibrium liquid-phase concentration of indigo carmine, respectively; V (litres) the volume of the solution and W (grams) the weight of each adsorbent. Experimental data were fit to different kinetics models like Lagergren, Elovich, and Ho and McKay using STATISTICA 6.0 software. pH data that were monitored before and after the experiments were 6.1 ± 0.6 for each measured time and each adsorbent material. If the adsorption process follows a first-order kinetic model (Lagergren), the velocity is proportional to the solute concentration and adsorption is preceded by diffusion through a boundary. This model is used for homogeneous materials and physical sorption. Adsorption kinetics and parameters of indigo carmine by all nanomaterials are shown in Fig. 4 and Table 2. The amount of dye adsorbed in the equilibrium is similar for bimetallic nanoparticles and C/Fe–Ni 75/25% composite (93.39 mg/g and 91.73 mg/g, respectively); however, the amount of dye adsorbed by C/Fe–Ni 95/5% composite was 80.9 mg/g. The kinetic constant shows that Fe–Ni nanoscale oxides removed

indigo carmine from the solution faster than composites. Correlation coefficient of this model shows higher value for the bimetallic system; this material can remove pollutants by physical sorption. Elovich model has been used properly in chemisorptions on highly heterogeneous materials. The desorption constants have similar values: 0.102, 0.076 and 0.099 mg/g for Fe–Ni system, C/Fe–Ni 75/25% and C/Fe–Ni 95/5%, respectively. Nevertheless, adsorption constant was higher for Fe–Ni nanoscale oxides; this proves the efficiency for removing indigo carmine. Regarding the correlation coefficient, the Elovich model shows higher values than those obtained with Lagergren model for both composites, which means that these materials follow a chemisorption mechanism. Pseudo-second-order kinetic parameters are also shown in Table 2. The amount of indigo carmine adsorbed in the equilibrium is similar for Fe–Ni nanostructures and C/Fe–Ni 75/25% composite (96.15 and 97.08 mg/g, respectively), comparable to those obtained by Lagergren model; however, the amount of dye adsorbed by C/Fe–Ni 95/5% composite was 92.59 mg/g. Also, the pseudo-second-order constant for Fe–Ni nanostructures (0.0081 g/mg h) is higher than that for C/Fe–Ni 75/25% and C/Fe–Ni 95/5% composites (0.0014 and 0.0010 g/mg h, respectively). The experimental data were best fitted to this model for the three adsorbent materials that were employed in this work having correlation coefficient values over 0.999; thus, Fe–Ni nanostructures and the two C/Fe–Ni

Table 3 Comparison of sorption capacities by different adsorbent materials for indigo carmine dye

Material	Dyestuff	Sorption capacity (mg/g)	References
Blast furnace sludge	Acid blue 113	2.1	Jain et al. (2003)
Modified silica	Acid blue 25	45.8	Phan et al. (2000)
Activated sewage sludge	Indigo carmine	60.04	Otero et al. (2003)
Pyrolyzed sewage sludge	Indigo carmine	30.82	Otero et al. (2003)
Activated clay	Acid blue 9	57.8	Ho et al. (2001)
Guava leaf powder	Basic blue 9	295	Ponnusami et al. (2008)
Spent tea leaves	Basic blue 9	300.05	Hameed (2009)
Metal hydroxide sludge	Reactive blue 19	275	Santos et al. (2008)
Fe-zeolitic tuff	Indigo carmine	32.83	Gutiérrez-Segura et al. (2009)
Carbonaceous material/HCl	Indigo carmine	92.83	Gutiérrez-Segura et al. (2009)
Fe–Ni nanoscale oxides	Indigo carmine	977.1	This work
C/Fe–Ni 75/25% composite	Indigo carmine	654.3	This work
C/Fe–Ni 95/5% composite	Indigo carmine	486.4	This work

Table 4 pH effect of indigo carmine by Fe–Ni nanostructures and C/Fe–Ni composites

Initial pH	pH and q_e values after indigo carmine contact					
	Equilibrium pH Fe–Ni	q_e (mg/g)	Equilibrium pH C/Fe–Ni 75/25%	q_e (mg/g)	Equilibrium pH C/Fe–Ni 95/5%	q_e (mg/g)
2	1.99	92.57	2.07	80.66	2.07	88.54
3	5.53	99.59	5.76	98.57	5.07	98.46
5	6.99	99.46	7.45	98.52	7.34	94.46
7	7.27	99.10	7.60	97.83	7.36	94.92
9	7.40	97.15	7.60	97.41	7.52	95.97
11	8.03	97.79	8.14	97.07	7.99	92.67
13	12.41	88.71	12.44	87.79	12.43	76.17

composites may have a heterogeneous surface. In addition, pseudo-second-order model suggests that chemisorption might be the rate-limiting step that controls these adsorption processes.

3.4 Isotherm Models

Different models have been developed for describing the behaviour of adsorbent materials adjusting to three different adsorption isotherms like Langmuir, Freundlich and Langmuir–Freundlich in order to correlate the equilibrium adsorption data using the STATISTICA 6.0 software. The different equation parameters of these models often provide insight into both the adsorption mechanism and the surface properties and affinity of the adsorbent. pH data monitored before and after the experiments were 6.0 ± 0.7 for each measured time and each adsorbent material. The Langmuir isotherm has been used by various researchers to study the sorption of a variety of compounds. This model describes a homogenous and uniform surface of materials forming a monolayer, and also considers that the sorption energy of each molecule is the same, independently of the surface of the material. Table 2 shows the isotherm parameters of dyestuff on the three adsorbent materials. The Fe–Ni nanostructures adsorption capacity was 977.18 mg/g, followed by C/Fe–Ni 75/25% composite with 654.33 mg/g, and a lower value, 486.41 mg/g, was obtained for C/Fe–Ni 95/5% composite, having correlation coefficient values of 0.93, 0.99 and 0.98, respectively. Table 3 (Gupta and Suhas 2009; Gutiérrez-Segura et al. 2009; Otero et al. 2003) shows different materials used in the removal of various blue dyes and its sorption capacity values. Indigo carmine removal

from aqueous solution has been evaluated by Otero et al. (2003) using activated sewage sludge (ASS) and pyrolyzed sewage sludge (PSS), where sorption capacity of ASS was 60.04 mg/g with 165 min of equilibrium time while sorption capacity of PSS was 30.82 mg/g and 180 min of equilibrium time. On the other hand, Gutiérrez-Segura et al. (2009) used Fe-zeolitic tuff and carbonaceous material from pyrolyzed sewage sludge treated with HCl, where the carbonaceous material from the pyrolysis of sewage sludge (sorption capacity 92.83 mg/g) was a better adsorbent for indigo carmine than the zeolitic material (sorption capacity, 32.83 mg/g). Hence, all adsorbent materials prepared and used in this work (Fe–Ni nanostructures and C/Fe–Ni composites) had much higher values of sorption capacity removing indigo carmine dyestuff from aqueous media in comparison to those obtained in previous works. The Freundlich

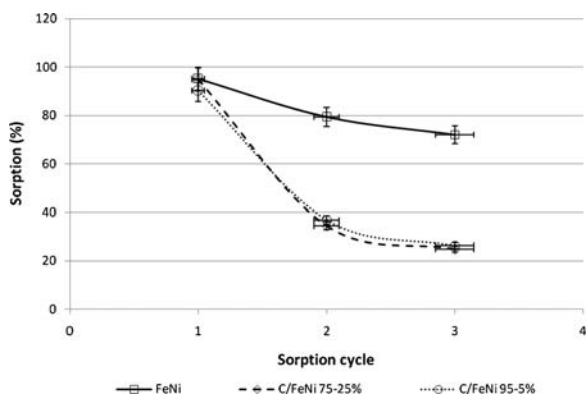


Fig. 5 Percentage of indigo carmine dye sorption compared to sorption–desorption processes using 30% H₂O₂ solution

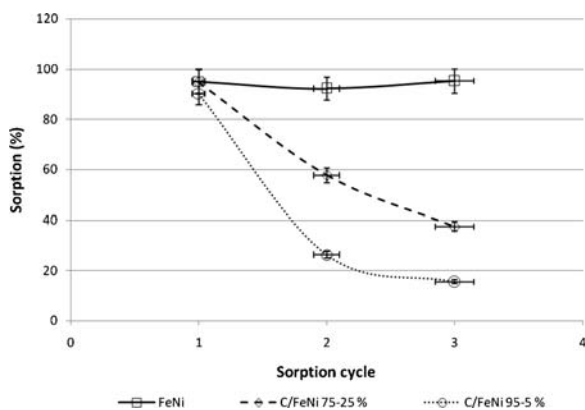


Fig. 6 Percentage of indigo carmine dye sorption compared to sorption–desorption processes using distilled water

isotherm is an empirical model employed to describe heterogeneous systems and multilayer adsorption. The model applies to adsorption on heterogeneous surfaces with interaction between adsorbed molecules. In all adsorbent materials, values of n are similar to each other. The reciprocal of these values are 0.477, 0.332 and 0.361 for Fe–Ni and C/Fe–Ni composites, respectively. This indicates that adsorption intensity is favourable according to Slejko (1985), implying, nevertheless, a heterogeneous surface structure. These values can be compared with those where Fe-zeolitic tuff ($n=0.66$) and carbonaceous material from pyrolyzed sewage sludge treated with HCl ($n=0.36$) were used by Gutiérrez-Segura et al. (2009) and to those where activated sewage sludge ($n=0.121$) and pyrolyzed sewage sludge (0.116) were employed by Otero et al. (2003). The Langmuir–Freundlich isotherm is a combination of Langmuir and Freundlich models. The experimental data were best fitted to this model for all adsorbent materials having correlation coefficient values over 0.99 for both composites; however, the correlation coefficient for Fe–Ni nanoscale oxides was 0.934. Similar results were obtained by Gutiérrez-Segura et al. (2009) using Fe-zeolitic tuff and carbona-

ceous material from pyrolyzed sewage sludge treated with HCl. Similarly, Dos Anjos et al. (2002) observed that both Langmuir and Freundlich models fitted indigo carmine adsorption on chitosan well, which indicated adsorption by combined mechanisms onto a heterogeneous surface.

3.5 Effect of pH

The pH of the dye solution plays an important role in the whole adsorption process and particularly on the adsorption capacity, influencing not only the surface charge of the adsorbent, the degree of ionization of the material present in the solution and the dissociation of functional groups on the active sites of the adsorbent but also the solution dye chemistry (Crini and Badot 2008). The effect of pH of indigo carmine on Fe–Ni nanostructures and C/Fe–Ni composites are presented in Table 4, where the pH values were considered as equilibrium pH values. The extent of removal was 95.8–98.8% in pH between 4 and 10 and decreased slightly at pH below 4 and above 10. pH behaviour could be explained by ionization of the adsorbate about pH 4, and the decrease of adsorption at pH 10 could be due to the presence of OH⁻ ions and the characteristics of the adsorbent. Table 4 shows that the equilibrium pH increases when the initial pHs are acid and decreases when the initial pHs are basic. This behaviour could be attributed to the properties of the neutral and dissociated species that behave as a weak acid and a strong base, respectively, and therefore there is less variation of pH when the initial pH value is closed to the pK_a of the dye, which is 7.74±0.22 (Gutiérrez 2011).

3.6 Sorption–Desorption Cycles

Figure 5 shows the percentage of indigo carmine dye sorption compared to sorption–desorption processes using 30% H₂O₂ solution. As it is observed, the dye

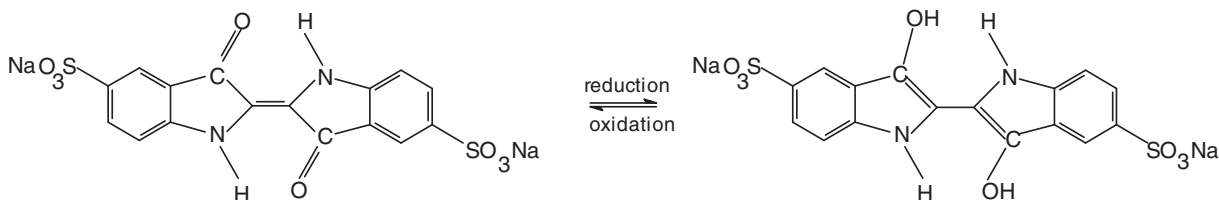


Fig. 7 Chemical structures of indigo carmine

sorption efficiency of all materials (FeNi oxides, C/FeNi 75/25% and C/FeNi 95/5%) decreases in each cycle (95%, 79.3%, 71.9%; 94.8%, 34.5%, 24.8%; and 90.2%, 36.8%, 26.2%, respectively); this behaviour occurs because the H₂O₂ solution may affect the chemical groups found on the surface of each material. Figure 6 shows the percentage of indigo carmine dye sorption compared to sorption–desorption processes using distilled water. As it is observed, the dye sorption efficiency of both composites (C/FeNi 75/25% and C/FeNi 95/5%) decreases in each cycle (94.8%, 57.6%, 37.4% and 90.2%, 26.2%, 15.4%, respectively); this behaviour was expected as these last samples contain carbonaceous material and it is probable that the removal of the dye takes place by a sorption mechanism. However, this behaviour is not observed for FeNi nanoscale oxides; the removal of this dye could take place by a redox mechanism (Fig. 7).

Finally, we compared also the content percentage of each metal (Fe and Ni) versus the maximum adsorption capacity of the dyestuff (q_0 , milligrams per gram) for all adsorbent materials. It can be observed that Fe has higher adsorption capacity than Ni. This, perhaps, can be because of the proportion of Fe in bimetallic nanostructures (75/25% Fe–Ni), composite C/Fe–Ni 75/25% which 25% was conformed by 75/25% Fe–Ni and other composite C/Fe–Ni 95/5% where 5% was 75/25% Fe–Ni. The same behaviour was observed with BET analysis.

4 Conclusions

Preparation of Fe–Ni nanostructures and novel C/Fe–Ni composites was achieved by a simple and cheap chemical reduction method, and the characterization was by TEM, SEM/EDS, XRD, BET and IR. All three tested materials removed indigo carmine from aqueous solutions in an efficient way. The experimental data of all adsorbents were adjusted to Ho and McKay kinetic model and Langmuir–Freundlich isotherm model, with results indicating chemisorptions on heterogeneous materials. Fe–Ni nanostructures have the higher adsorption capacity accordingly to Langmuir isotherm model. Moreover, adsorption capacity for removal of indigo carmine by three nanomaterials was efficient in pH between 4 and 10 having 95.8–98.8% of dye removal but decreased slightly at pH below 4 and above 10. Before three sorption–desorption cycles,

sorption efficiency of both composites decreases in each cycle, but this behaviour is not observed for FeNi nanoscale oxides. In addition, the sorption capacities of materials are proportional to the content of metals and therefore their specific area.

Acknowledgements Authors are grateful to Jorge Pérez del Prado (Instituto Nacional de Investigaciones Nucleares) and Francisco Ruiz (Centro de Nanociencia y Nanotecnología-Universidad Nacional Autónoma de México) for technical support on SEM/EDS and XRD, respectively.

References

- Baldrian, P., Merhautova, V., Jir, G., Nerud, F., Stopka, P., Hruby, M., et al. (2006). Decolorization of synthetic dyes by hydrogen peroxide with heterogeneous catalysis by mixed iron oxides. *Environmental*, *66*, 258–264.
- Banat, I. M., Nigam, P., Singh, D., & Marchant, R. (1996). Microbial decolorization of textile-dye-containing effluents. *Bioresource Technology*, *58*, 217–227.
- Bokare, A. D., Chikate, R. C., Rode, C. V., & Paknikar, K. M. (2007). Effect of surface chemistry of Fe–Ni nanoparticles on mechanistic pathways of azo dye degradation. *Environmental Science and Technology*, *41*, 7437–7443.
- Crini, G. (2006). Non-conventional low-cost adsorbents for dye removal: a review. *Bioresource Technology*, *97*, 1061–1085.
- Crini, G., & Badot, P. M. (2008). Application of chitosan, a natural aminopolysaccharide, for dye removal from aqueous solutions by adsorption processes using batch studies: a review of recent literature. *Progress in Polymer Science*, *33*, 399–447.
- Dos Anjos, F. S. C., Vieira, E. F. S., & Cestari, A. R. (2002). Interaction of indigo carmine dye with chitosan evaluated by adsorption and thermochemical data. *Journal of Colloid and Interface Science*, *253*, 243–246.
- Forgacs, E., Cserhati, T., & Oros, G. (2004). Removal of synthetic dyes from wastewaters: a review. *Environment International*, *30*, 953–971.
- Guivarch, E., Trevin, S., Liáte, C., & Oturan, M. A. (2003). Degradation of azo dyes in water by electro-Fenton process. *Environmental Chemistry Letters*, *1*, 38–44.
- Gupta, V. K., & Suhas. (2009). Application of low-cost adsorbents for dye removal—a review. *Journal of Environmental Management*, *90*, 2313–2342.
- Gutiérrez, S. E. E., (2011). *Remoción de azul índigo y cadmio presentes en soluciones acuosas empleando un material zeolítico modificado y un material carbonoso activado*. Tesis Doctoral, Facultad de Química, Toluca, México. UAEMéx.
- Gutiérrez-Segura, E., Solache-Ríos, M., & Colín-Cruz, A. (2009). Sorption of indigo carmine by a Fe-zeolitic tuff and carbonaceous material from pyrolyzed sewage sludge. *Journal of Hazardous Materials*, *170*, 1227–1235.
- Hameed, B. H. (2009). Spent tea leaves: a new non-conventional and low-cost adsorbent for removal of basic dye from aqueous solutions. *Journal of Hazardous Materials*, *161*, 753–759.

- Ho, Y. S., Chiang, C. C., & Hsu, Y. C. (2001). Sorption kinetics for dye removal from aqueous solution using activated clay. *Separation Science and Technology*, *36*, 2473–2488.
- Jain, A. K., Gupta, V. K., Bhatnagar, A., & Suhas. (2003). Utilization of industrial waste products as adsorbents for the removal of dyes. *Journal of Hazardous Materials*, *101*, 31–42.
- Kunwar, P. S., Mohan, D., Sinha, S., Tondon, G. S., & Gosh, D. (2003). Color removal from wastewater using low-cost activated carbon derived from agricultural waste material. *Industrial and Engineering Chemistry*, *42*, 1965–1976.
- Liao, Q., Tannenbaum, R., & Wang, Z. L. (2006). Synthesis of FeNi₃ alloyed nanoparticles by hydrothermal reduction. *The Journal of Physical Chemistry B*, *110*, 14262–14265.
- Ma, L. M., Ding, Z. G., Gao, T. Y., Zhou, R. F., Xu, W. Y., & Liu, J. (2004). Discoloration of methylene blue and wastewater from a plant by a Fe/Cu bimetallic system. *Industrial Chemosphere*, *55*, 1207–1212.
- Mc Callum, J. E. B., Madison, S. A., Sibel, A., Depinto, R. L., & Rojas, W. R. U. (2000). Analytical studies on the oxidative degradation of the reactive textile dye uniblue A. *Industrial Environmental Science and Technology*, *34*, 5157–5164.
- Mittal, A., Mittal, J., & Kurup, L. (2006). Batch and bulk removal of hazardous dye, indigo carmine from wastewater through adsorption. *Journal of Hazardous Materials*, *137 B*, 591–602.
- Otero, M., Rozada, F., Calvo, L. F., Garcia, A. I., & Moran, A. (2003). Elimination of organic water pollutants using adsorbents obtained from sewage sludge. *Dyes and Pigments*, *57*, 55–65.
- Phan, T. N. T., Bacquet, M., & Morcellet, M. (2000). Synthesis and characterization of silica gels functionalized with monochlorotriazinyl beta-cyclodextrin and their sorption capacities towards organic compounds. *Journal of Inclusion Phenomena and Macrocyclic Chemistry*, *38*, 345–359.
- Ponnusami, V., Vikram, S., & Srivastava, S. N. (2008). Guava (*Psidium guajava*) leaf powder: novel adsorbent for removal of methylene blue from aqueous solutions. *Journal of Hazardous Materials*, *152*, 276–286.
- Robinson, T., Chandran, B., & Nigam, P. (2002). Removal of dyes from a synthetic textile dye effluent by biosorption on apple pomace and wheat straw. *Water Research*, *36*, 2824–2830.
- Santos, S. C. R., Vilar, V. J. P., & Boaventura, R. A. R. (2008). Waste metal hydroxide sludge as adsorbent for a reactive dye. *Journal of Hazardous Materials*, *153*, 999–1008.
- Slejko, F. L. (1985). *Adsorption technology: a step-step approach to process evaluation and application*. New York and Basel: Marcel Dekker Inc.
- Slokar, Y. M., & Le Marechal, A. M. (1998). Methods of decoloration of textile wastewaters. *Dyes and Pigments*, *37*, 335–336.
- Tee, Y., Grulke, E., & Bhattacharyya, D. (2005). Role of Ni/Fe nanoparticle composition on the degradation of trichloroethylene from water. *Industrial English Chemistry Research*, *44*, 7062–7070.
- Torres-Pérez, J., Solache-Rios, M., & Colín-Cruz, A. (2008). Sorption and desorption of dye remazol yellow onto a Mexican surfactant-modified clinoptilolite-rich tuff and a carbonaceous material from pirólisis of sewage sludge. *Water, Air, and Soil Pollution*, *187*, 303–313.
- Trujillo-Reyes, J., Sánchez-Mendieta, V., Colín-Cruz, A., & Morales-Luckie, R. (2010). Removal of Indigo Blue in aqueous solution using Fe/Cu nanoparticles and C/Fe–Cu nanoalloy composites. *Water, Air, and Soil Pollution*, *207*, 307–317.
- Vautier, M., Guillard, C., & Herrmann, J. M. (2001). Photocatalytic degradation of dyes in water: case study of indigo and of indigo carmine. *Catalysis*, *201*, 46–59.
- Walker, G. M., & Weatherle, L. R. (1997). Adsorption of acid dyes on to granular activated carbon in fixed beds. *Water Research*, *31*, 2093–2101.
- Wang, X., Zhu, N., & Yin, B. (2008). Preparation of sludge-based activated carbon and its application in dye wastewater treatment. *Journal of Hazardous Materials*, *153*, 22–27.
- White, R. J., Luque, R., Budarin, V. L., Clark, J. H., & Macquarrie, D. J. (2008). Supported metal nanoparticles on porous materials. Methods and applications. *Chemical Society Reviews*, *38*(2), 481–494.
- Zhang, W. X. (2003). Nanoscale iron particles for environmental remediation: an overview. *Journal of Nanoparticle Research*, *5*, 323–332.